

On variable geometric factor systems for top-hat electrostatic space plasma analyzers

Glyn A Collinson^{1,2} and Dhiren O Kataria¹

¹ Mullard Space Science Laboratory, Holmbury St Mary, UK

² Heliophysics Science Division, NASA Goddard Spaceflight Center, Greenbelt, MD, USA

E-mail: gac@mssl.ucl.ac.uk

Received 19 April 2010, in final form 13 July 2010

Published 13 August 2010

Online at stacks.iop.org/MST/21/105903

Abstract

Even in the relatively small region of space that is the Earth's magnetosphere, ion and electron fluxes can vary by several orders of magnitude. Top-hat electrostatic analyzers currently do not possess the dynamic range required to sample plasma under all conditions. The purpose of this study was to compare, through computer simulation, three new electrostatic methods that would allow the sensitivity of a sensor to be varied through control of its geometric factor (GF) (much like an aperture on a camera). The methods studied were inner filter plates, split hemispherical analyzer (SHA) and top-cap electrode. This is the first discussion of the filter plate concept and also the first study where all three systems are studied within a common analyzer design, so that their relative merits could be fairly compared. Filter plates were found to have the important advantage that they facilitate the reduction in instrument sensitivity whilst keeping all other instrument parameters constant. However, it was discovered that filter plates have numerous disadvantages that make such a system impracticable for a top-hat electrostatic analyzer. It was found that both the top-cap electrode and SHA are promising variable geometric factor system (VGFS) concepts for implementation into a top-hat electrostatic analyzer, each with distinct advantages over the other.

Keywords: variable geometric factor, space plasma analyzer, electrostatic analyzer, electron spectrometer

1. Introduction

1.1. 'Top-hat' electrostatic analyzers

In space, electrons are incident upon a spacecraft over a range of velocities (energies) and from any direction in the sky (4π sr). 'Top-hat' electrostatic analyzers [1, 2] select charged particles that meet specific energy and angular criteria, and 'image' their exit position according to incident azimuth. Their purpose is to build up a six-dimensional phase-space distribution, $f(x, y, z, v_x, v_y, v_z)$, of the electrons by scanning through 4π and over an energy range typically of 1 eV to ≈ 30 keV.

Energy selection of electrons is achieved with a pair of nested hemispherical electrodes, the 'inner hemisphere' and the grounded 'outer hemisphere' (see figure 1). When a voltage is applied to the inner hemisphere, an electric field is created between the hemispheres. Charged particles must follow the curvature of the electrostatic analyzer plates in order to be detected. The 'top hat' (or 'top cap') is a third nested hemispherical grounded electrode, positioned above the aperture. The half-angle subtended by the inner hemisphere is known as the 'truncation angle', and the half-angle subtended by the top hat/top cap is known as the 'top-hat angle' as shown in figure 1. Many top-hat analyzers additionally use a collimator. The azimuthal field of view of a top-hat analyzer is typically either 360° or 180° .

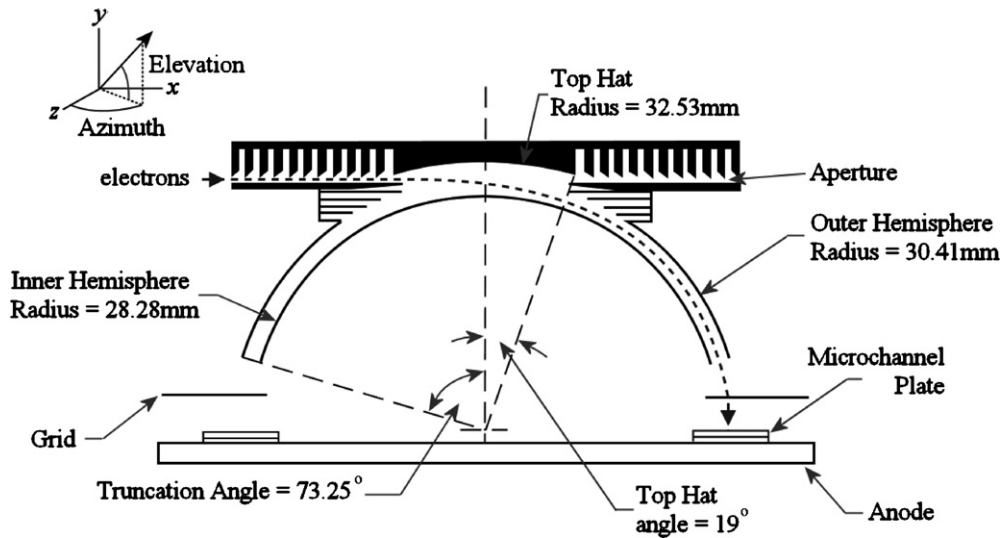


Figure 1. Schematic of a typical ‘top-hat’ electrostatic analyzer (dimensions are those of the improved plasma analyzer used in this study).

Particles within the acceptance bandpass of the instrument will traverse the deflection region and strike a micro-channel plate (MCP) [3]. The MCP acts much like a photomultiplier tube, creating an electron shower upon electron incidence that is detected as a charge deposition on an anode by read-out electronics. The anode is often sub-divided into segments, giving the instrument azimuthal sensitivity. A voltage is usually applied to the front of the MCP to increase the detection efficiency by accelerating the incident charged electrons onto the surface. This necessitates the placement of a grounded grid between the MCP and the hemispheres in order to electro-optically isolate these two regions.

1.2. Instrument parameters

An electrostatic analyzer accepts charged particles over a range of bandpasses. Energy and angular bandpasses are well established in the literature [1, 4]. In this paper, we also discuss the lesser known ‘impact parameter’ bandpass, which was discovered to be of vital importance to top-hat analyzers with variable geometric factor systems (VGFS).

The impact parameter is the perpendicular distance between the velocity vector of an incoming electron and the centreline of the instrument (*z*-axis). If electrons are fired into the collimator with an increasing impact parameter, there will reach a point at which none will be accepted (see figure 2). Therefore, just as electrons are accepted over a bandpass of energy and elevation, electrons are also accepted over a range of impact parameters, or over an ‘impact parameter bandpass’.

The performance of an analyzer is described by several parameters, each of which will now be briefly introduced. The first important characteristic of the instrument is the K-factor (also often referred to as the *analyzer constant*). The K-factor (*k*) is given by equation (1), where E_0 is the peak of the accepted energy bandpass, *q* is the charge of the charged particle and *V* is the voltage applied to the inner hemisphere:

$$\frac{E_0}{q} = kV \tag{1}$$

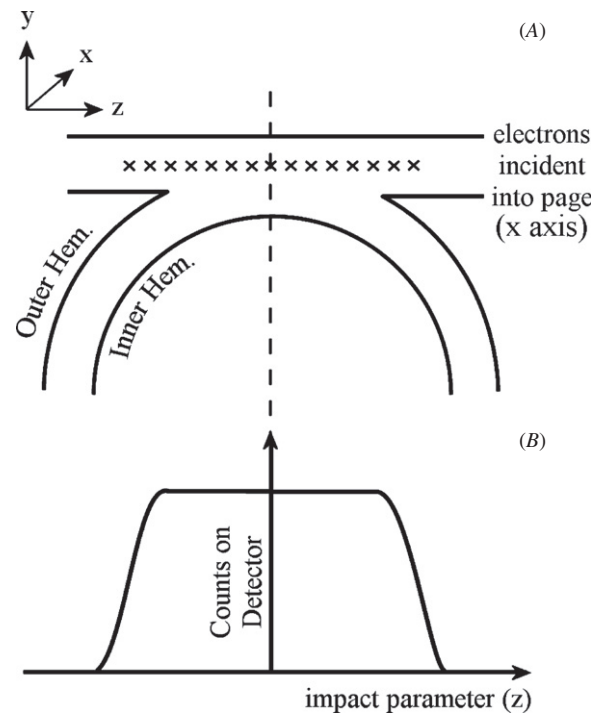


Figure 2. (A) Illustration of the cross-section of a simplified top-hat analyzer, electron beam incident into the page. (B) Illustration of the ‘impact parameter bandpass’.

Another important value is the energy resolution. The energy resolution of the analyzer is defined as the full width at half-maximum (FWHM) of the energy pass-band (ΔE) divided by the peak of the energy pass-band (E_0), as given by equation (2):

$$\text{Energy resolution} = \frac{\Delta E}{E_0} \tag{2}$$

A top-hat electrostatic analyzer has a bandpass of elevation acceptance approximating to a Gaussian [1]. The peak of the acceptance bandpass is referred to as the peak

elevation (θ_0). In an ideal case, the peak of the elevation bandpass should be oriented along the x - z axis of the aperture (0°):

$$\text{Peak elevation} = \theta_0 \quad (3)$$

The FWHM of the elevation bandpass is referred to as the elevation resolution ($\Delta\theta$):

$$\text{Elevation resolution} = \Delta\theta. \quad (4)$$

1.3. Geometric factor

1.3.1. Definition. The geometric factor (GF) of a top-hat analyzer is an instrument parameter that relates the number of electrons detected to the number incident upon the instrument [4]. The GF is, therefore, a measure of the sensitivity of a top-hat electrostatic analyzer. An accurate determination of the GF is essential to accurately determine particle flux or the distribution function of the particles being measured, from which properties such as density and temperature can be calculated. In this study, the GF was calculated using a modified version of the equation proposed by Johnstone and co-workers [5] (see equation (5) below) for use in laboratory calibration:

$$\text{GF} = \frac{eA_F}{I_0T} \Delta v' \Delta\psi \Delta\phi' N_{\text{MCP}} Q. \quad (5)$$

Here, e is the charge of an electron, A_F is the area of electron acceptance, $\Delta v'$ is the velocity step (converted to energy step), $\Delta\psi$ is the elevation step between measurements, $\Delta\phi'$ is the azimuthal step, I_0 is the beam current, T is the acquisition time, N_{MCP} is the number of electrons hitting the MCP and Q is the detector efficiency. The simulations in this study have assumed the detector to be 100% efficient ($Q = 1$) because detection efficiency is dependent on the type of system used and also the energy of electrons under study [6].

1.3.2. The need for a variable geometric factor. Saturation will occur to the detector if the number of particles striking the surface exceeds a critical rate [7]. For the PEACE sensors [8] currently in the orbit aboard the Cluster [9] and Double Star [10] spacecraft, this is $\approx 3 \times 10^6$ counts per second. Due to very large variations in the dynamic range of the space plasma flux [11], sensors with a fixed GF must be targeted toward specific plasma populations. Sensors designed to have a high level of charged particle throughput to operate in regions of tenuous plasma such as the terrestrial magnetotail will become saturated in regions occupied with denser populations, such as in Earth's magnetosheath.

One solution to this problem is to have an instrument with several separate sensors, each possessing different GFs. An example of this is the PEACE instrument with a factor of 3.65 difference in the GF between two sensors (HEEA and LEEA). Each sensor is optimized to study a different region of the Earth's magnetosphere. Another approach is the cluster ion spectroscopes CODIF and HIA sensors [12], both of which have two separate (180° azimuthal) apertures on the same top-hat electrostatic sensor. This traditional approach of flying separate sensors with different sensitivities, however, requires

additional mass and power. An alternative lower resource intensive solution to this problem would be a common analyzer design with the capability of varying electron throughput through variation of the GF. Although there do exist other kinds of space plasma analyzers with VGFS [13], the methods employed are unsuitable for the widely used top-hat analyzer.

1.4. Method of computer simulation

A full description of our tool kit can be found in [14]. Ray tracing calculations were performed by a commercially available package, SIMION 8.0, and its output is analyzed using a series of IDL routines. Simulated electrons are launched stochastically toward the aperture over the whole range of energy, angle and area acceptances of the sensor. SIMION calculates the trajectory of each electron through the instrument using standard numerical techniques. The output of SIMION is analyzed in a series of specially written IDL data analysis routines which plots the response of the analyzer as well as calculating the GF, k , θ_0 , $\frac{\Delta E}{E_0}$ and $\Delta\theta$. All the data points presented in this study represent the mean of ten simulations, with error bars showing the standard deviation. The spatial resolution of the geometry in this study is $7.8125 \mu\text{m}$, or 128 grid points per mm. Given the breadth of this study, simulations were limited to a single common voltage setting of the inner hemisphere (150 V), approximating to a 1 keV electron energy.

This tool kit has been validated through its successful use in the assistance of the ground calibration of the Mars Express and Venus Express ASPERA [15] electron spectrometer [14], and also in the in-flight calibration of the Cassini CAPS [16] electron spectrometer [17].

1.5. Outline

This paper is outlined as follows. A discussion of possible VGFS can be found in section 2. The results of our computer simulations can be found in section 3 with a discussion in section 4. Conclusions, including a summary of the optimum VGFS methods, can be found in section 5.

2. Variable geometric factor systems

2.1. Overview of simulated solutions

This paper describes the computational study of three different methods of implementation of an electrostatic VGFS into a 'top-hat' electrostatic analyzer. In this study, the first of its kind, all methods have been designed around a common analyzer head, so that each method can be fairly compared. The baseline analyzer used is the improved plasma analyzer (IPA), a prototype sensor based on the PEACE LEEA [8] with all dimensions reduced by a factor of $\sqrt{2}$. The instrument parameters and electron optical properties of the sensor are close to that of LEEA, but with the GF reduced by half. The three methods studied are as follows.

- (1) Inner filter plates,
- (2) split hemispherical analyzer and

(3) top-cap electrode.

The novel filter plate method (section 2.2) employs a pair of deflection plates after the hemispherical energy deflection region to radially defocus the beam. The beam is ‘flared’ to either side of the detector, and thus less electrons are detected. The second method, currently under development for the Bepi Colombo Mercury Magnetospheric Orbiter [18, 19], is that of a split inner hemisphere. The third method is the application of an electric potential to the top cap. Both of these last two techniques use the same method to reduce the GF, splitting the analyzer into two separate regions with an independently controlled acceptance bandpass. By diverging the voltages applied to these electrodes, the overall bandpass of the whole instrument is reduced. This is the first study to discuss inner filter plates and a top-cap electrode system. This is also the first study to describe the generalized properties of a split hemispherical analyzer (SHA).

2.2. Inner filter plates

The first method of altering the GF of the instrument was through the addition of an extra pair of electrostatic deflection plates between the energy analysis region (hemispheres) and the MCP (see panel A, figure 3). These shall be referred to as ‘filter plates’. When a voltage is applied to the filter plates, the electron beam defocuses along the radial axis of the analyzer (the azimuthal effect is negligible). Whilst the electrons near the centre of the energy bandpass still strike the MCP, those at the fringes will strike the filter plates and are rejected. Further electron rejection can be achieved through the use of an annular MCP such as that on PEACE, or a smaller anode under the MCP which has a smaller radial coverage than the striking electron beam. The filter plates can thus defocus the beam to be wider than the detector, increasing the rejection at the fringes of the energy bandpass.

An immediately obvious advantage of this method is that the VGFS filter plates could be separated from the energy selection region with an extra grounded grid (‘upper grid’, panel A, figure 3). This means that the peak of the energy bandpass, and thus the K-factor of the instrument should be largely unchanged by operation of the filter plates. This greatly reduces the complexity of the calibration process.

2.3. Split hemispherical analyzer

Top-hat plasma analyzers accept charged particles over a range of energy (E), elevation (θ), impact parameter (z) and over the width of the aperture/collimator (y , see figure 1). The performance of the instrument is governed by how much of this four-dimensional space is sampled at any given moment. We shall refer to this as the overall (or total) acceptance bandpass of the instrument, $A(E, \theta, z, y)$.

A top-hat plasma sensor is composed of two deflection regions: The top-cap region (‘top-hat r1’, figure 1) and the outer-hemisphere region (‘outer hemisphere r2’, figure 1). Each of these regions has a different 4D acceptance bandpass ($A_{\text{top hat}}$ and $A_{\text{outer hem.}}$, respectively). The overall acceptance bandpass of the sensor is a convolution of the

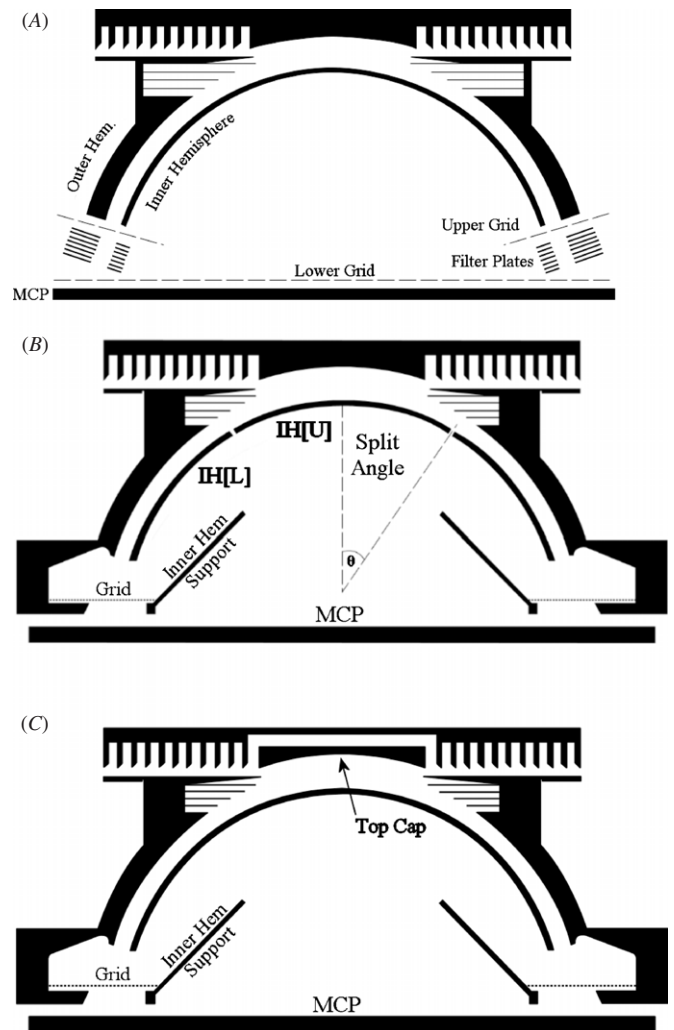


Figure 3. (A) Filter plates, (B) split hemispherical analyzer, (C) top-cap analyzer.

output of the two. In the case of the SHA, the instrument is further divided into independently controlled regions by splitting the inner hemisphere along a ‘split angle’ (see panel B, figure 3). The voltages applied to each segment can be independently controlled, allowing independent control of the energy bandpass in each region. In this study, the two segments of the inner hemisphere will be referred to under the following nomenclature.

- (1) IH[U]—upper segment of the inner hemisphere.
- (2) IH[L]—lower segment of the inner hemisphere.

For a SHA, the total acceptance bandpass is a convolution of the 4D acceptances of IH[U] and IH[L]. Diverging the voltages applied to IH[U] and IH[L] will diverge the peak of the energy bandpasses of these two regions. The more the peaks are diverged, the lesser the overlap between the energy bandpasses of each segment, and thus the overall acceptance bandpass of the entire instrument, $A(E, \theta, z, y)$, is reduced, resulting in fewer electrons striking the MCP.

An illustration of this can be seen in figure 4. The top panel shows the separate energy bandpasses for different applied voltages of the upper segment (IH[U]—dotted line, figure 4)

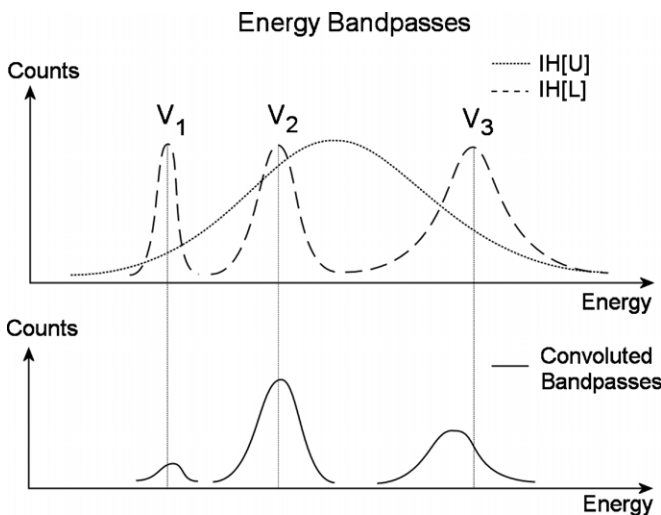


Figure 4. Illustration of the convolution of energy bandpasses (solid line, lower panel) from the upper segment of the inner hemisphere (IH[U], dotted line, upper panel) and the lower segment of the outer hemisphere (IH[L], dashed line, upper panel) when three different voltages are applied to IH[L].

and the lower segment (IH[L]—dashed line, figure 4). The lower panel of figure 4 shows the *overall convolved energy bandpass* (solid line) of the whole instrument as observed at the MCP, i.e. the overall energy bandpass, $A(E)$, of the sensor as defined by the overlap between the energy acceptance bandpasses of IH[U] and IH[L].

The energy bandpass of IH[U] is much broader than that of IH[L] because the separation between electrodes in the top-hat region is larger and the angle subtended in the top-hat region is smaller in the top-hat region, meaning that electrons are accepted over a wider range of energies. As the voltage on the lower segment IH[L] is increased ($V_1 > V_2 > V_3$, shown in figure 4), the peak and FWHM of the acceptance bandpass of IH[L] also increases.

When voltages V_1 and V_3 are applied to IH[L], there is little overlap with the energy bandpass of the IH[U] and thus the convolved energy bandpass (lower panel, figure 4) is reduced. Since the area under the overall energy bandpass has been reduced, fewer electrons strike the MCP and thus the GF is reduced. Another important thing to note is that the convolved energy bandpass may no longer be a Gaussian distribution, and depends on the selected GF, as in the idealized case for a classic non-split top-hat analyzer.

There are two possible modes of operation of an SHA. One is to keep the voltage on IH[U] (upper section) of the inner hemisphere constant and vary the voltage on IH[L] (lower section). The second is the opposite: keep the voltage on the IH[L] constant and vary the voltage on IH[U]. Since the bandpasses of the upper and lower segments are not identical, the response is different under either mode of operation.

For each mode of operation, the voltages applied to one segment relative to another can be either increased or decreased. In this study, we shall discuss this in terms of the *ratio* of voltage applied to each of the segments. There are three key questions to answer for the design of an SHA:

(1) What is the optimal split angle of the inner hemisphere?

- (2) On which part of the hemisphere is the voltage to be varied, upper (IH[U]) or lower (IH[L])?
- (3) Does an increased or decreased voltage provide the best overall instrument performance?

The IPA analyzer was simulated with a split hemisphere with split angles of 10° , 19° (top-cap angle), 30° , 40° , 50° and 60° , covering the whole range of possible split angles over the truncation angle of the analyzer (73.25°).

2.4. Top-cap electrode

A top-cap electrode VGFS works on exactly the same principle as an SHA. The energy deflection region is divided into two sections, each with an independently controlled electric potential. However, instead of splitting the inner hemisphere, voltages are applied directly to the top cap of the analyzer (see panel C, figure 3). If the voltage on the inner hemisphere is kept constant, positive voltages on the top cap will reduce the potential difference in the top cap/inner hemisphere region, whereas negative voltages will increase the potential difference. Therefore, the total acceptance bandpass observed at the MCP will be a convolution of the bandpasses of the top cap/inner hemisphere region and the inner/outer hemisphere regions.

3. Results

3.1. Inner filter plates

The results in this section are from simulations of the filter plate geometry shown in panel A, figure 3. This geometry represents the culmination of a systematic study of different shapes of plate as shown in figure 5. Each shape of plate was simulated with both a disk and an annular MCP. Full details of these results are not presented here for the sake of brevity, given that filter plates were ultimately rejected as a viable VGFS concept. One key finding of the study was that filter plates need to be compact to minimize the azimuthal defocusing of the electron beam on the MCP if there is too great a separation between the deflection region and the detector.

These early designs featured elongated filter plates, in order to increase the amount of electron deflection for a given voltage on the plates. However, longer plates were abandoned after it was discovered that the volume envelope required for such a system forces the MCP to be moved further away from the focal point of the analyzer. The result of this is that the azimuthal resolution of the simulated instrument became unacceptably poor, with the electron beam spreading out to occupy as much as a 10° – 20° arc of the detector (rather than the optimal focused point). Therefore, any filter plate system must be made to be compact enough so that the detector does not have to be moved down and away from the focal point of the instrument. This led to the development of the miniaturized filter plates as shown in panel A of figure 3.

In this paper, we discuss voltages in terms of '*voltage ratios*'. For filter plates, this is defined by equation 6, where V_{FP} is the voltage on the filter plates and V_{IH} is the voltage on the inner hemisphere (kept constant). In this study, we have

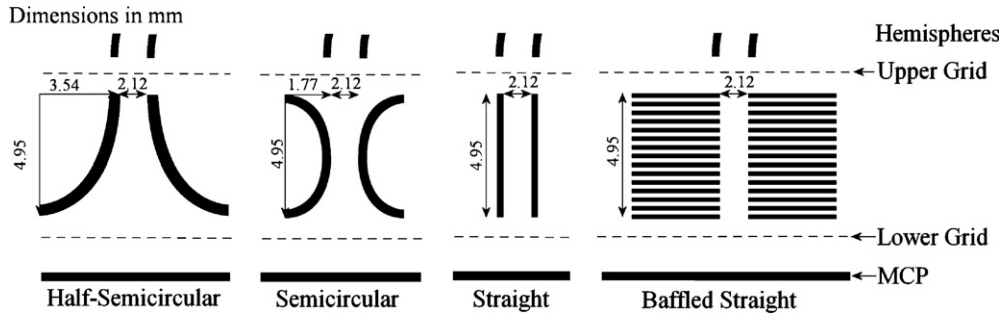


Figure 5. The four shapes of the filter plate investigated in this study.

chosen V_{IH} to be 150 V. Given that the K-factor (analyzer constant) of the IPA is 6.2, this equates to $E_0 \approx 1$ keV.

$$\text{Voltage ratio}_{(\text{Filter plate studies})} = \frac{V_{FP}}{V_{IH}}. \quad (6)$$

3.1.1. MCP footprint. The azimuthal spread of the electron beam striking the MCP determines the azimuthal acceptance of the analyzer. Panel A of figure 6 shows the variation of the FWHM of azimuthal cross-section of the electron beam as voltages are applied to the filter plates. Whilst the flaring of the electron beam will cause an increase in the radial component of the beam profile, it has little effect in the azimuthal component. This is excellent, since this means that the electron beam will not spread out over multiple anode segments, and the azimuthal resolution of the instrument will be conserved.

3.1.2. Geometric factor. The change in the normalized GF can be seen in panel B of figure 6. Applying a voltage difference of 3.5 to the filter plates causes an $\approx 50\%$ drop in the GF for an analyzer where the fringes of the energy bandpass are diverted onto either side of an annular MCP (solid red line), and only an $\approx 80\%$ drop in the GF for a disk MCP where all the electrons exiting the filter plates strike the detector. It is clear, therefore, that a significant factor in filter plate electron rejection comes from the defocusing of the electron beam to either side of the MCP. This $\approx 50\%$ rejection rate is fairly typical at this voltage ratio when compared to the other geometries of filter plates that were investigated. It is then clear that in order to gain even the factor of 4 difference in the GF between the PEACE LEEA and HEEA, significant potentials must be applied to the filter plates. This would make filter plates very resource intensive and also at risk of catastrophic failure through high-voltage breakdown [20].

3.1.3. Energy resolution ($\frac{\Delta E}{E_0}$). The variation in energy resolution can be seen in panel C of figure 6. The $\Delta E/E$ for the case of the annular MCP (dotted red line) is significantly lower than that of the disk MCP (solid red line). This is due to the fact that the fringes of the energy bandpass physically strike outside the active area of the annular MCP. As the voltages on the filter plates are increased, the energy resolution improves ($\Delta E/E$ decreases), as the fringes of the bandpass are further rejected.

3.1.4. K-factor (analyzer constant). One significant advantage of filter plates is that the peak of the energy bandpass remains unaffected, as long as the plates are designed to be symmetric with the beam. This results in a constant K-factor, as shown in panel D of figure 6. This is important, since it means that the measured energy is independent of the voltage applied to the filter plates ($E_0/q = kV$).

3.1.5. Elevation bandpass. The grids separating filter plates from the inner hemisphere electron-optically isolate the VGFS from the rest of the analyzer. The result of this is that the elevation bandpass is unaffected by voltages applied to the sensor. This is a highly attractive feature of a filter plate system, since the peak elevation (panel F, figure 6) and elevation resolution (panel E, figure 6) remain unchanged.

3.2. Split hemispherical analyzer

In this section, we report key results from our electron-optical simulations of our systematic study of the SHA. Energy and impact parameter bandpass are discussed for all six split angles and both modes of operation (variation of the voltage on IH[U] and variation of the voltage on IH[L]). Thereafter, we concentrate specifically on two split angles, representative of each mode of operation.

For an SHA, the voltage ratio is defined by equation (7), where $V_{IH(\text{varied})}$ is the voltage on the segment of the inner hemisphere (IH[U] or IH[L]) being varied and $V_{IH(\text{constant})}$ is the voltage on the segment of the inner hemisphere kept constant. In this study, we have chosen $V_{IH(\text{constant})}$ to be 150 V:

$$\text{Voltage ratio}_{(\text{SHA})} = \frac{V_{IH(\text{varied})}}{V_{IH(\text{constant})}} \quad (7)$$

Thus, when the voltage ratio is 1.0, the performance of the instrument is the same as that for a classic un-split top-hat electrostatic analyzer. Given that the K-factor (analyzer constant) of the IPA is 6.2, this equates to $E_0 \approx 1$ keV.

3.2.1. Energy bandpass

Variation of IH[U]. Figure 7 shows the variation in energy bandpass as the voltage on IH[U] is varied, and the voltage on IH[L] is kept constant. All six split angles are shown. At a split angle of 10° , there is little variation in the overall bandpass since the angle subtended by IH[L] \gg IH[U]. The

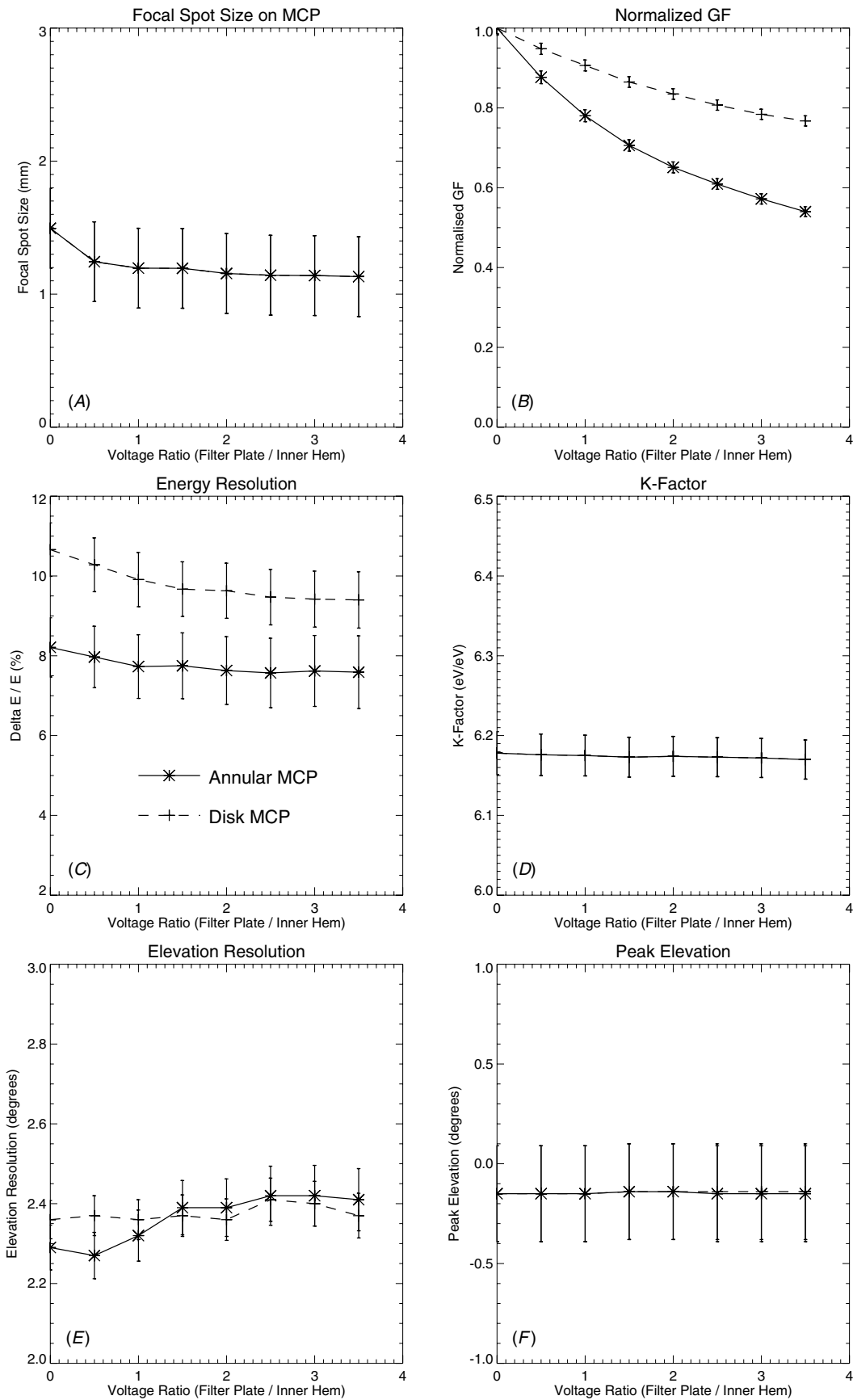


Figure 6. Performance of an IPA analyzer with inner filter plates. Errors are approximate, representing our best understanding.

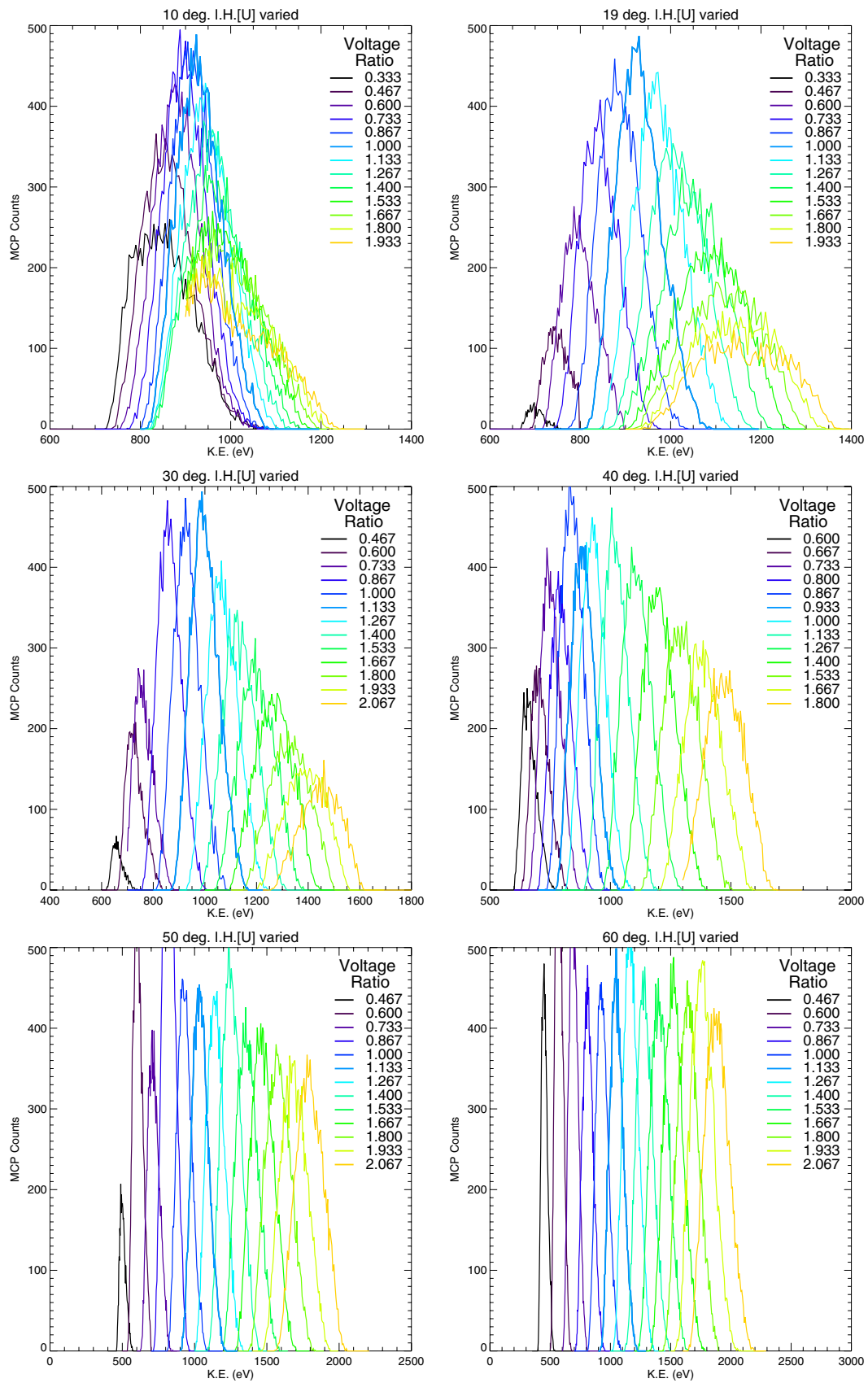


Figure 7. The energy bandpasses of a split hemispherical IPA analyzer, with a variety of split hemispherical truncation angles, variation of IH[U].

total convolved bandpass is, therefore, completely dominated by IH[L], and even at the extreme simulated voltage ratios (0.3, 2), the total electron throughput cannot be made to drop by even the factor of 3.65 difference required between the PEACE LEEA and HEEA sensors.

The opposite is true at 60° (bottom-right panel, figure 7), where the angle subtended by IH[U] \gg IH[L]. The height and shape of the total energy bandpass behaves much as it would if the instrument was a classic un-split hemispherical top-hat analyzer. Therefore, at very large and very small split angles, it is shown that the instrument performance will approximate to the un-split case. This is exactly as one would expect. Based purely on variation in energy bandpass, there exists an optimum split angle at approximately half the truncation angle (in this case, $\geq 19^\circ$ and $\leq 40^\circ$).

Variation of IH[L]. Figure 8 shows the variation in energy bandpasses for all six split angles with the voltage on IH[U] kept constant, and the voltage on IH[L] varied. At 10°, there is little variation in the energy bandpass. At 60°, the angle subtended by IH[U] \gg IH[L] and variations of the voltage ratio have a negligible effect. Even for a split angle of 50°, it is not possible to significantly cut off all electron throughput. Therefore, one important conclusion of this study is that there is no advantage in split truncation angles either less than the top-cap angle or close to the overall truncation angle of the hemispheres (in this case, 73.25°).

For the case of splitting the hemispheres along the 19° top-cap angle, it is still clearly possible to have a dramatic effect on the overall electron throughput. Since in this case the angle subtended by IH[L] is greater than that subtended by IH[U], the energy range over which the bandpass is altered is much larger when operating in this mode, than when IH[L] is kept constant and IH[U] is varied.

3.2.2. Impact parameter bandpass. Figure 9 shows the variation in impact parameter bandpass for a range of voltage ratios, when the voltage on IH[U] is varied and the voltage on IH[L] is kept constant. The figure is sub-divided into twelve panels in two columns and six rows. Panels in the left-hand column show the variation in impact parameter bandpass for voltage ratios less than 1, whereas panels in the right-hand column show voltage ratios greater than 1. Among the six rows each show a different split angle, increasing from 10° to 60°, top to bottom.

First, consider the case of voltage ratios less than 1 (left column, figure 9). Decreasing the voltage on IH[U] relative to IH[L] causes the area under the impact parameter bandpass to decrease. As the voltage ratio is decreased, the fringe fields become more important and the shape changes from an approximate square function with a well-defined cutoff between $z = \pm 6$ mm and ± 8 mm to a curve with a poorly defined cutoff. Therefore, the instrument would have a variable sensitivity over the impact parameter.

This is, however, still preferable to the alternative of increasing the voltage ratio to be >1 (see figure 9, right column). As the voltage difference is increased, the centre of the impact parameter bandpass appears to become ‘eroded’,

until at a voltage ratio of ≈ 2 (shown in red), the bandpass has adopted a clear ‘double peak’ structure. Therefore, electrons input along the centreline of the instrument are rejected. Electrons reaching the MCP come from two separate populations, each of which will have a separate focal spot on the anode. This is highly undesirable.

As with the energy bandpass, the impact parameter bandpass is in actuality a convolution of the two acceptance bandpasses of IH[U] and IH[L]. The reason for this double peaked distribution is that the paths of acceptance closest to the centreline of the instrument are governed by IH[U] whilst the paths furthest away are governed by IH[L]. In the case of voltage ratios > 1 , IH[U] is rejecting the majority of incoming electrons, whilst IH[L] (with voltages set closer to the peak of the overall acceptance bandpass) is letting electrons through to strike the MCP. Therefore, electrons passing further away from the centerline of the instrument are more likely to be accepted. Therefore, IH[U] is taking a ‘bite’ out of the acceptance over impact parameter.

The overall topology of the impact parameter bandpasses is very similar when the voltage on IH[L] is varied and the voltage on IH[U] is kept constant (and has been omitted for brevity), with the important exception that voltage ratios < 1 will now cause double peaked impact parameters. This is because the only electrons that can strike the MCP must be accepted by IH[L], but for voltage ratios < 1 , electrons near the centreline of the instrument are rejected by IH[U]. Therefore, the following generalized rules must be obeyed when operating an SHA.

- Voltage ratios > 1 must be used for variations of voltage on IH[U].
- Voltage ratios < 1 must be used for variations of voltage on IH[L].

From here on we shall discuss the relative performances of two SHA concepts that represent the optimal split angles for the IPA analyzer under both of the above two modes of operation.

- (1) 19° split angle. Voltage on IH[U] varied (ratios < 1).
- (2) 30° split angle. Voltage on IH[L] varied (ratios > 1).

3.2.3. Electron beam focusing. One of the key advantages of a top-hat analyzer geometry is that the inner/outer hemispheres focus parallel rays of electrons onto the detector [1] for a certain deflection angle. It is of vital importance that any VGFS system does not dramatically defocus the electron beam at the MCP, or the azimuthal resolution will be impacted. Figure 10 shows simplified SIMION simulations for visualization purposes of the electrostatic focusing of a 30° SHA. Projections of the electron paths through the VGFS are displayed. Parallel rays of electrons (red) are fired into the page. When the voltage ratio is 1 (center panel), electrons follow the curvature of the hemispheres and are focused onto the grid. This is exactly the same as for the PEACE LEEA analyzer. Recall that ‘double peaked’ impact parameter bandpasses are observed for voltage ratios > 1 when the voltage on IH[U] is varied (as in the right-hand column of figure 9), but are observed for voltage ratios < 1 when the

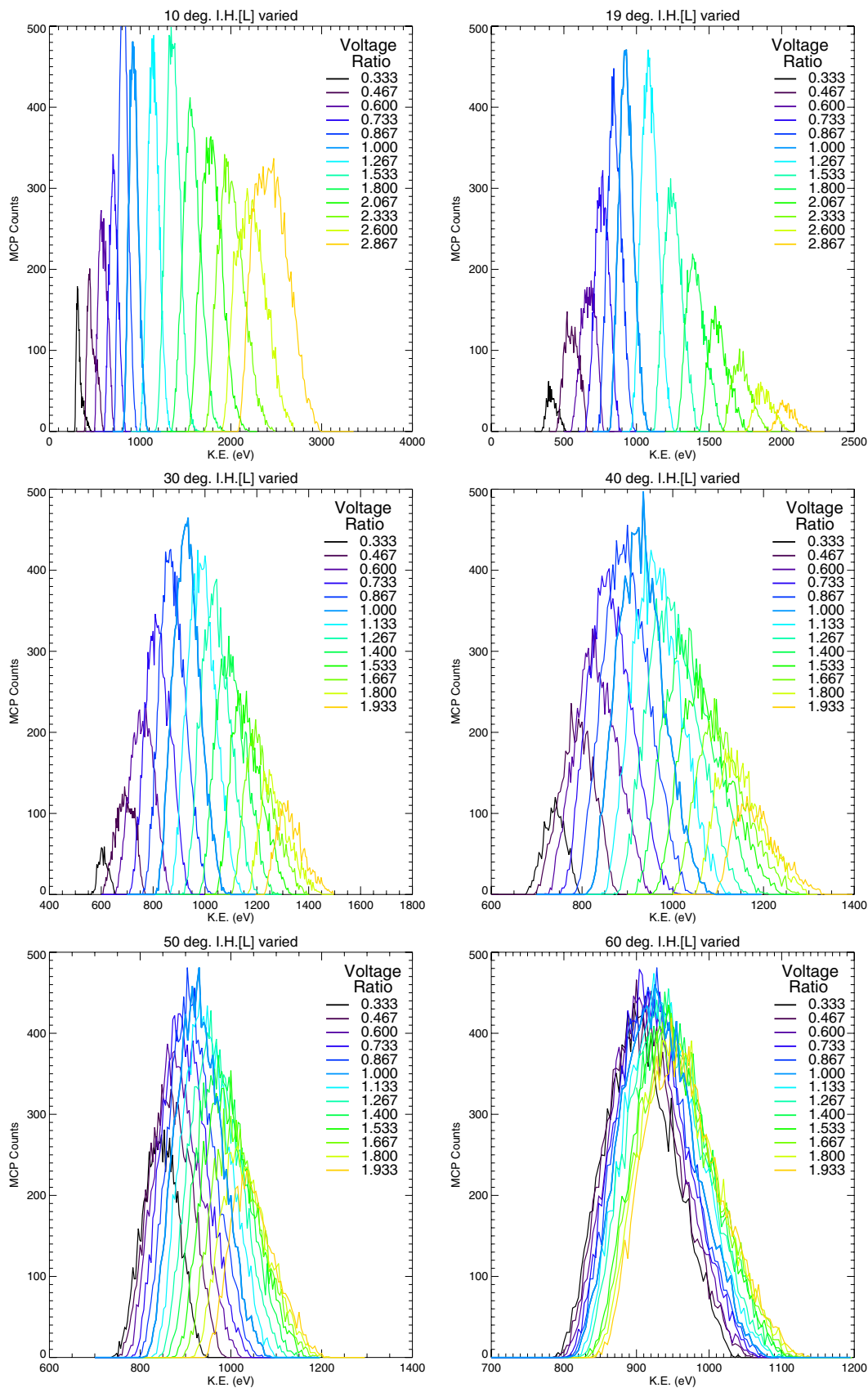


Figure 8. The energy bandpasses of a split hemispherical IPA analyzer, with a variety of split hemispherical truncation angles, variation of IH[L].

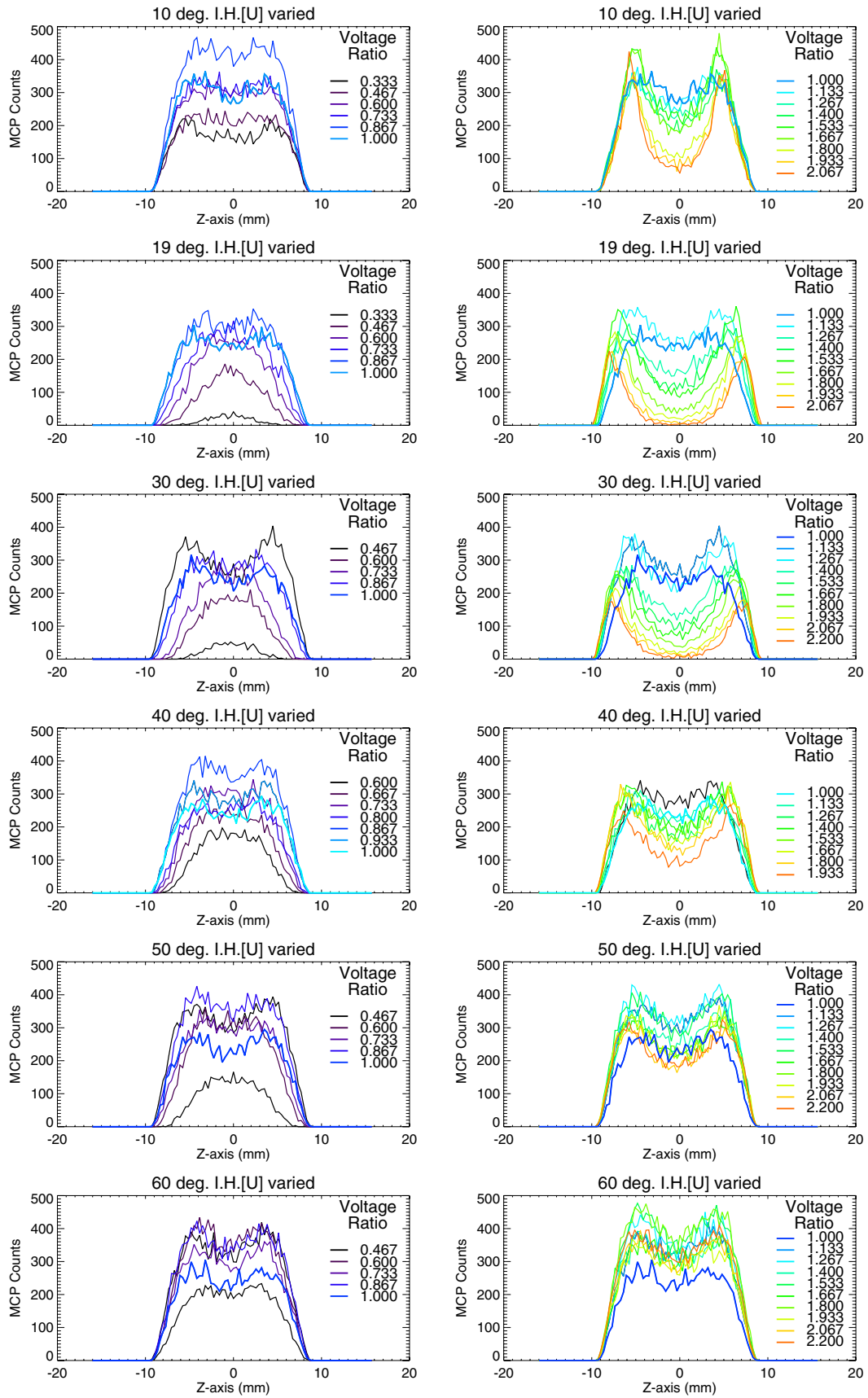


Figure 9. The impact parameter bandpasses of a split hemispherical IPA analyzer, with a variety of split hemispherical truncation angles, variation of IH[U].

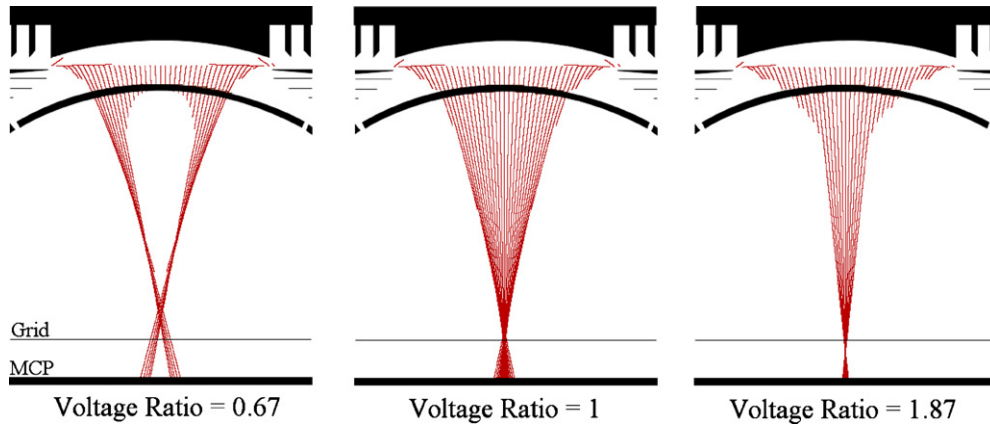


Figure 10. Simulated electron beam focusing properties of a 30° SHA when the voltage on IH[L] is varied with voltage ratios < 1, =1 and >1.

voltage on IH[L] is varied. In this case, IH[L] is being varied, so the later case is true.

The disadvantages of a ‘double peaked’ impact parameter bandpass can be seen in the left panel of figure 10 (voltage ratio 0.67). Electrons incident down the centerline of the instrument are rejected whilst electrons at the fringes are accepted, forming two separate spots on the MCP. This is undesirable because it will dramatically affect the azimuthal resolution of the instrument.

In the case of voltage ratios > 1 for variations of IH[L], and therefore for variations of IH[U], <1, the fringes of the impact parameter bandpass are rejected. The result of this is to reduce the range of impact parameters over which electrons are accepted, and therefore reduce the size of the electron beam at the MCP (right-hand panel, figure 10).

Cross-sections of the simulated beam were taken on the MCP, and the variation in the FWHM of the beam profile can be seen in panel A of figure 11 (19°—black, 30°—blue). It is shown that an optimized SHA will reduce the size of the focal spot as the VGFS system is activated. There is little difference in performance between an SHA in either of the case.

3.2.4. Geometric factor. The variation in the GF can be seen in panel B of figure 11. The case where IH[U] is varied is shown in black (19° split angle), and the case where IH[L] is varied is shown in blue (30° split angle). Both show a similar reduction in the GF of at least an order of magnitude. This does not necessarily represent a limit to the possible extent of reduction, but simply the point at which simulations were terminated. The reduction in GF is not linear with the voltage ratio because the rejection mechanism is based on the diverging overlap of the Gaussian-like energy bandpasses of the different regions of the analyzer (recall figure 4).

3.2.5. Energy resolution ($\frac{\Delta E}{E_0}$). The energy resolution (figure 11, panel C) is initially constant, but then decreases as voltage ratios diverge from unity. In general, as long as the split angle is approximately half the truncation angle and the analyzer is not producing ‘double peaked’ impact parameter bandpasses, the energy resolution, $\Delta E / E$, will decrease (i.e. improve) as the GF is reduced.

3.2.6. Peak of energy bandpass (E_0). One critical difference between the variation of IH[U] (19°—black) and IH[L] (30°—blue) in an SHA is that higher voltage ratios mean a higher E_0 (see the black line, top panel, figure 4). Therefore, to sample a particular energy of space plasma, the overall voltages required will be lower, and the entire sensor is less resource intensive (this is the equivalent to having a higher analyzer constant for a classic un-split hemispherical analyzer). Therefore, in this regard, there is a clear advantage in keeping the voltage on IH[U] constant whilst increasing the relative voltage on IH[L].

3.2.7. Elevation bandpass. The variation in peak elevation can be seen in panel F of figure 11, and the FWHM of the elevation bandpass can be seen in panel E of figure 11. As the voltages on IH[U] and IH[L] are diverged, the peak is shifted toward the physical $\approx \pm 2^\circ$ limit of field of the view as defined by the aperture. This causes the FWHM of the elevation bandpass to shrink as it is physically obstructed. Although the elevation resolution is dependent on the design of the analyzer, it is important to note that a change to the elevation bandpass is unavoidable, whatever the geometry of the SHA.

3.3. Top cap electrode

In this section, the term ‘voltage ratio’ refers to the ratio of voltage between the top cap (V_{TC}) and on the inner hemisphere (V_{IH}) (see equation 8). For the sake of consistency between the three VGFS concepts, we have chosen V_{IH} to be 150 V, equating to an acceptance, $E_0 \approx 1$ keV. Unlike an SHA, it is possible for a top-cap VGFS analyzer to have voltage ratios of zero when no voltages are applied to the top cap. This is equivalent to a voltage ratio of 1 for an SHA.

$$\text{Voltage ratio}_{\text{Top cap studies}} = \frac{V_{TC}}{V_{IH}} \quad (8)$$

In general, the effect of applying a voltage to the top cap on the energy and impact parameter bandpasses is consistent with that of a 19° SHA (and have not been printed here for the sake of brevity). For electrons, it was found that positive voltages must always be used while operating a top-cap analyzer, as negative voltages resulted in a ‘double peaked’

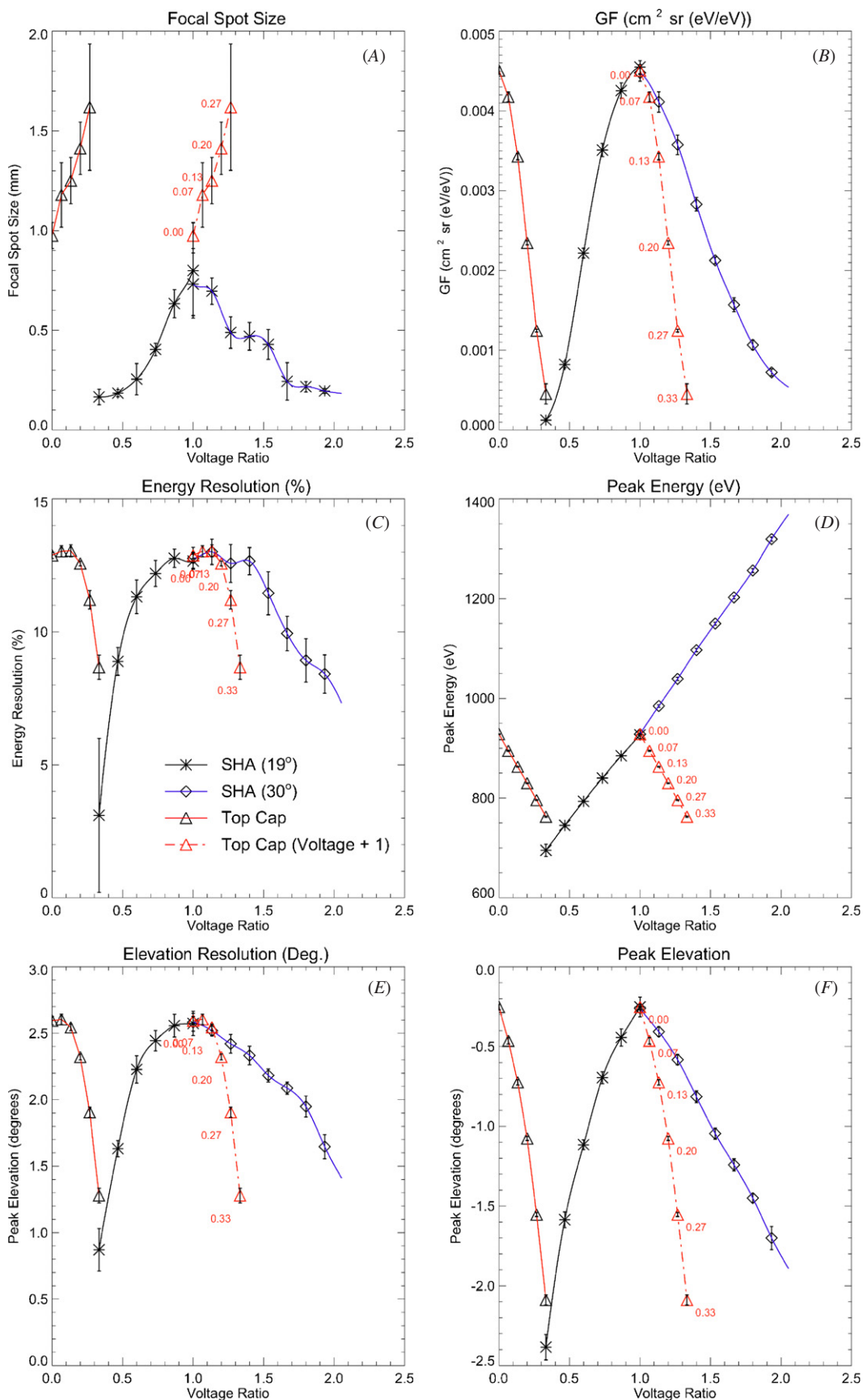


Figure 11. Variation in instrument performance for an optimized SHA with voltage on IH[U] varied (black—19° split angle) and voltage on IH[L] varied (blue—30° split angle). The performance of the IPA with a top-cap electrode is shown in red and repeated with the voltage ratio +1 for comparison with the SHA (dotted red line).

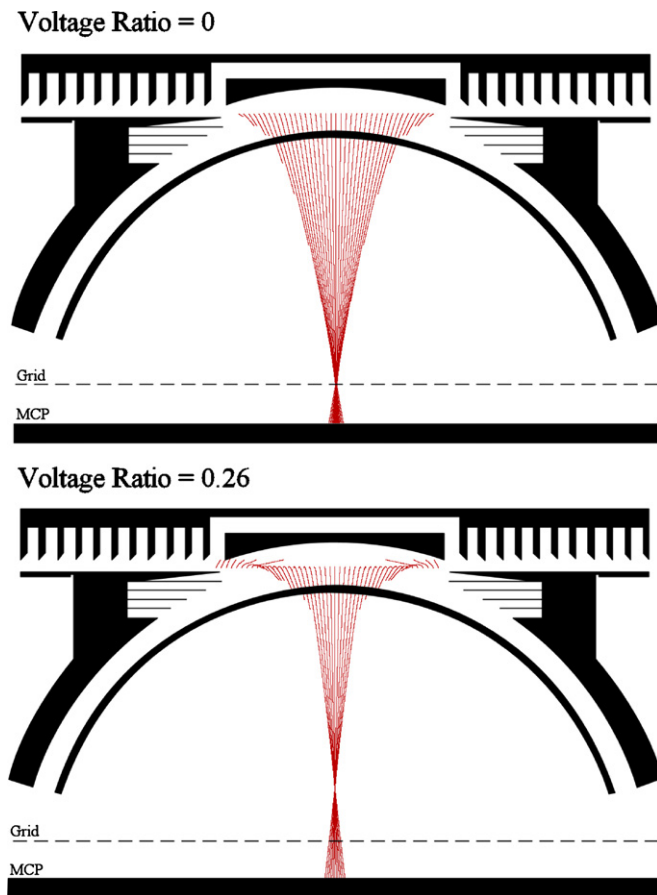


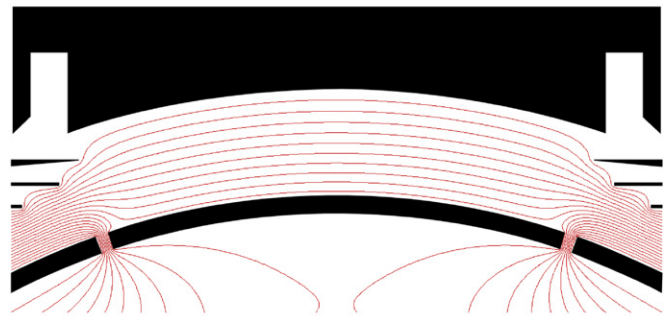
Figure 12. SIMION simulation of the focusing properties of a top-cap electrode VGFS, showing the case of no voltage on top cap (top panel) and a voltage ratio of 0.26 (bottom panel).

impact parameter bandpass. As with the 19° SHA (black), the peak (panel D, figure 11) and FWHM (panel C, figure 11) of the energy bandpass decrease as voltages are applied to the top cap.

3.3.1. Focal spot size. The size of the focal spot on the MCP can be seen in panel A of figure 11 (red line). For ease of comparison with an SHA, all the top-cap data sets have been repeated with a +1 shift in the voltage ratio (dotted red line, the actual voltage ratio marked next to each data point). Applying a voltage to the top cap causes the size of the focal spot on the MCP to increase. This will have an adverse effect on the azimuthal resolution of the instrument. Note that this is unlike an SHA, where the focal spot size becomes smaller as the GF is reduced.

Figure 12 shows a ray-tracing of a parallel beam of electrons incident into the page (generated in SIMION) in a similar format to figure 10. In the case where no voltages are applied to the top cap (top panel), the hemispheres focus the electron beam at the grid. When a voltage is applied to the top cap (bottom panel), the focal length of the analyzer decreases. Thus, the focal point moves upward and the beam diverges further by the time it strikes the MCP. For the IPA, this represents an increase from the beam occupying $\approx 2^\circ$ arc to

Split Hemisphere



Top Cap

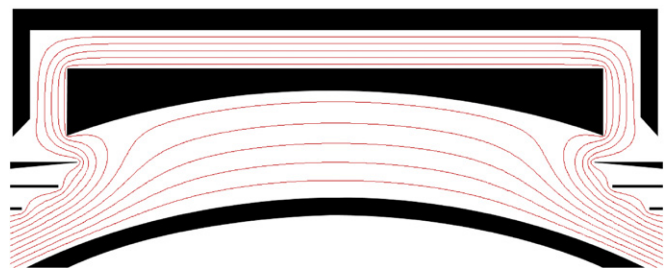


Figure 13. SIMION simulation of the lines of electric field equipotential inside an SHA (top panel) and a top-cap VGFS (bottom panel).

occupying $\approx 4^\circ$ arc. This will adversely affect the azimuthal resolution of the instrument.

3.3.2. Geometric factor. The variation of the GF of a top-cap analyzer is consistent with that of an SHA (red line—figure 12, panel B). This is unsurprising given that the operational principle of a top-cap analyzer is similar to that of a SHA. The key difference, however, is that the same reduction in the GF can be achieved with a voltage ratio difference of ≈ 0.3 , as compared to a voltage ratio of ≈ 0.6 for a 19° SHA with variation of IH[U] (black) and ≈ 1 for a 30° SHA with variation of IH[L] (blue).

3.3.3. Elevation bandpass. As with energy bandpass, the magnitude of the change in elevation bandpass is consistent with that of a 19° SHA (variation IH[U]). The peak (panel F, figure 11) shifts toward the $\approx \pm 2^\circ$ limit of field of view of the analyzer, and the FWHM (panel E, figure 11) shrinks through this physical obstruction. However, this change is achieved with a lesser increase in the voltage ratio. To understand this, it is important to consider the penetration of the electric field into the aperture. Figure 13 shows a SIMION simulation of this, with contours of the electric field equipotential lines shown in red. The electric field generated by the top-cap electrode (bottom panel) penetrates much further into the aperture than in the case of the SHA (top panel). Therefore, although operation of either a SHA or a top cap will cause a shift in the peak of the elevation bandpass, this is much more prevalent in the later. This physical obstruction of the elevation bandpass also accounts for the rapid decrease in the GF, as the acceptance is

shifted outside of the physical field of view of the sensor, as defined by the geometry of the aperture.

4. Discussion

4.1. Inner filter plates

Based purely on this electron optical study, miniaturized filter plates seem a promising concept in that the GF can be reduced, whilst the K-factor and angular (elevation) resolution remain unaffected. The initial problem of a poor azimuthal resolution with longer filter plates was overcome by miniaturizing the plates and keeping the MCP near the focal point of the analyzer. However, two other major factors must be taken into account in the consideration of the viability of inner filter plates.

4.1.1. Secondary electron contamination. In order to effectively reduce the GF with inner filter plates, the main rejection mechanism is the divergence of the electron beam so that a good proportion of electrons fall outside the active area of the MCP. High energy primary electrons striking the metal surfaces on either side of the annular MCP will generate secondary electrons [21, 22]. Assuming an aluminum surface, the secondary electron yield will be close to 1 for primary electrons of 200 eV or greater [23]. The secondary electrons generated in this region will strike the MCP, leading to significant contamination. Mitigating this would be a significant challenge, presenting a major drawback for this concept.

4.1.2. High voltage breakdown. For the filter plate geometry considered here, three and a half times the voltage on the inner hemisphere must be applied to achieve a factor of 2 reduction in the GF (see panel B, figure 6). This is insufficient, for example, when compared to the current factor of 3.65 difference in the GF between the PEACE HEEA and LEEA sensors [8]. As these high voltages would be required to be applied over very small gaps between electrodes, the risk of high voltage breakdown [20] causing irreparable damage to the instrument is significantly high.

4.2. Split hemispherical analyzer

An SHA offers a number of advantages over the 'internal filter plate' concept described in section 2.2. The GF can be reduced by at least an order of magnitude, compared to a factor of only 2 with filter plates for the same applied voltage. The voltage differences required are, therefore, far less for a given reduction in the GF, making an SHA less resource intensive and less prone to catastrophic failure due to voltage breakdown. Another advantage of splitting the inner hemisphere over adding filter plates is the fact that this method does not require a significant increase in the mass or volume envelope. However, for an SHA, all instrument parameters are altered along with the GF, and the analyzer must be re-calibrated for each voltage setting. Given that this is the current practice for traditional solutions involving multiple sensors with different sensitivities, this is not seen as a major

disadvantage. In general, a key finding of this study is that all instrument parameters improve as the GF is reduced.

Although the optimal split angle will be dependent on the specific analyzer geometry, the results of this study strongly suggest that in general, this will lie at approximately half the total truncation angle of the hemispheres. For the IPA, this was $\approx 30^\circ$. The optimum performance was obtained when the voltage on IH[U] was kept constant, and the voltage on IH[L] was increased (voltage ratios > 1).

One of the possible concerns with an SHA is that of voltage breakdown between the two segments of the inner hemisphere. Therefore, the lower the voltages required, the lesser the risk of high voltage breakdown and the smaller the gap required between the two sections of the inner hemisphere. Assuming a maximum electron energy of ≈ 30 keV for a 30° SHA (cf PEACE ≈ 26.4 keV), the maximum voltage required would be ≈ 2800 V for IH[U] and ≈ 5600 V for IH[L]. Under typical engineering guidelines (1 kV per mm), this potential difference would dictate a separation of ≈ 2.8 mm between the segments of the inner hemisphere, larger than the 2.1 mm separation between the hemispheres and fringe-field effects inside the energy deflection region of the analyzer will become significant. When implementing an SHA, this engineering guideline must be intelligently re-evaluated through careful design practices in order to reduce the risk of voltage breakdown whilst minimizing the impact on the electron optics.

4.3. Top cap electrode

Compared to the SHA, a top-cap electrode has several advantages over that of an SHA. It provides a greater decrease in the GF for a given voltage difference and the overall variation in instrument performance is reduced. Additionally, the elevation and energy resolutions are improved as the GF is lowered.

However, one key disadvantage of the top-cap geometry simulated here is the defocusing of the electron beam at the MCP. In our analyzer, this degraded the azimuthal resolution by a factor of ≈ 2 . This can have a significant effect on instrument performance and must be carefully considered when selecting a VGFS system.

5. Conclusions

The purpose of this study was to compare three different methods of implementing a VGFS into a top-hat electrostatic analyzer: inner filter plates, SHA and top-cap electrode. All three systems were simulated as a part of a common analyzer head so that their relative merits could be fairly compared.

Filter plates have the important advantage that they facilitate the reduction in instrument sensitivity whilst all other instrument parameters remain constant. However, filter plates have numerous disadvantages that make such a system challenging to implement.

Both the top cap and SHA were found to be the promising concepts, and are largely comparable in their abilities to reduce the GF. The operational principles of an SHA and top-cap

electrode system are the same. The instrument is divided into two or more regions, in which the electric potential can be independently controlled. The overall performance of the instrument is the result of a convolution of the bandpasses of the different regions inside the analyzer. The GF is reduced by diverging the energy bandpasses of these regions.

After an extensive study of a range of different truncation angles and modes of operation of an SHA, the optimal split angle, was found to be at approximately half of that of the truncation angle. The best performance was achieved by keeping the voltage on the upper segment of the inner hemisphere (IH[U]) constant, and by increasing the voltage on the lower segment (IH[L]). The key advantage of this method when compared to increasing the voltage on a top-cap electrode is that it gives a higher peak energy (E_0) for a given voltage ratio, meaning that the voltages used in the SHA instrument overall can be reduced. The main disadvantage of an SHA is that caution must be taken in the design of the analyzer to ensure that voltage breakdown does not occur between the segments of the hemispheres.

A top-cap VGFS shares many of the positive attributes of an SHA, chiefly in that the energy and elevation resolution both improve as the GF is lowered. A top cap also has the additional advantage over an SHA that less of a voltage difference is required in order to achieve the same reduction in the GF. However, a distinct disadvantage of a top-cap system is the degradation to azimuthal resolution caused by the divergence of the electron beam at the MCP.

In conclusion, both the top-cap electrode and SHA were found to be promising VGFS concepts for implementation into a top-hat electrostatic analyzer. Both systems have shown distinct advantages and disadvantages over the other. However, as with the design of all space plasma instrumentation, the selection of a VGFS should ultimately be driven by the operational requirements and the geometry of the instrument in question.

Acknowledgments

This work was supported by UK Science and Technology Facilities Council studentship funding. The authors wish to thank Rudy Frahm for assistance in preparing the manuscript, and Robert Beddington for his input on optimizing our simulation method.

References

- [1] Carlson C W, Curtis D W, Paschmann G and Michel W 1982 An instrument for rapidly measuring plasma distribution functions with high resolution *Adv. Space Res.* **2** 67–70
- [2] Sablik M J, Golimowski D, Sharber J R and Winningham J D 1988 Computer simulation of a 360° field of view ‘top-hat’ electrostatic analyzer *Rev. Sci. Instrum.* **59** 146–55
- [3] Wiza J L 1979 Microchannel plate detectors *Nucl. Instrum. Methods* **162** 587–601
- [4] Wuest M, Evans D S and Von Steiger R 2007 Calibration of particle instruments in space physics *ISSI Scientific Report SR-007*
- [5] Johnstone A D *et al* 1987 The Giotto three-dimensional positive ion analyser. *J. Phys. E Sci. Instrum.* **20** 795–805
- [6] Bordoni F 1971 Channel electron multiplier efficiency for 10–1000 eV electrons *Nucl. Instrum. Methods* **97** 405
- [7] Fraser G W, Pain M T, Lees J E and Pearson J F 1991 The operation of microchannel plates at high count rates *Nucl. Instrum. Methods Phys. Res.* **306** 247–60
- [8] Johnstone A D *et al* 1997 Peace: a plasma electron and current experiment *Space Sci. Rev.* **79** 351–98
- [9] Escoubet C P, Schmidt R and Goldstein M L 1997 Cluster—science and mission overview *Space Sci. Rev.* **79** 11–32
- [10] Liu Z X, Escoubet C P, Pu Z, Laakso H, Shi J K, Shen C and Hapgood M 2005 The Double Star mission *Ann. Geophys.* **23** 2707–12
- [11] Baumjohann W and Treumann R A 1997 *Basic Space Plasma Physics* (London: Imperial College Press)
- [12] Rème H *et al* 2001 First multispacecraft ion measurements in and near the Earth’s magnetosphere with the identical Cluster ion spectrometry (CIS) experiment *Ann. Geophys.* **19** 1303–54
- [13] Moore T E *et al* 1995 The thermal ion dynamics experiment and plasma source instrument *Space Sci. Rev.* **71** 409–58
- [14] Collinson G A, Kataria D O, Coates A J, Tsang S M E, Arridge C S, Lewis G R, Frahm R A, Winningham J D and Barabash S 2009 Electron optical study of the Venus Express ASPERA-4 electron spectrometer (ELS) top-hat electrostatic analyser *Meas. Sci. Technol.* **20**
- [15] Barabash S *et al* 2006 The analyzer of space plasmas and energetic atoms (ASPERA-3) for the Mars Express mission *Space Sci. Rev.* **126** 113–64
- [16] Young D T *et al* 2004 Cassini plasma spectrometer investigation *Space Sci. Rev.* **114** 1–4
- [17] Lewis G R *et al* 2010 In-flight calibration of the Cassini–Huygens CAPS electron spectrometer *Planet. Space Sci.* **58** 427–36
- [18] Sauvaud J-A, Fedorov A, Aoustin C, Medale J-L, Rouzaud J, Le Comte E and Saito Y 2008 The Mercury Electron Analyzers (MEA) for Bepi Colombo: variable geometric factor spectrometers *37th COSPAR Scientific Assembly (COSPAR, Plenary Meeting vol 37)* p 2749
- [19] Saito Y, Sauvaud J A, Hirahara M, Barabash S, Delcourt D, Takashima T and Asamura K 2010 (BepiColombo MMO/MPPE Team) Scientific objectives and instrumentation of Mercury Plasma Particle Experiment (MPPE) onboard MMO *Planet. Space Sci.* **58** 182–200
- [20] Meek J M and Craggs J D 1978 *Electrical Breakdown of Gases* (New York: Wiley)
- [21] Bruining H 1954 *Physics and Applications of Secondary Electron Emission* (Oxford: Pergamon)
- [22] Baragiola R A 1991 *Current Topics in Kinetic Electron Emission from Solids in Interactions of Charged Particles with Solids and Surfaces* (New York: Plenum)
- [23] Bruining H and de Boer J H 1938 Secondary electron emission: Part I. secondary electron emission of metals *Physica* **5** 17